

Physical modeling of conduction and switching in chalcogenide glasses

Daniele Ielmini, Andrea L. Lacaita

Dipartimento di Elettronica e Informazione, Politecnico di Milano, piazza L. da Vinci 32, 20133 Milano, ielmini@elet.polimi.it

ABSTRACT

The paper addresses recent progresses in the physical understanding of the sub-threshold conduction and threshold switching in chalcogenide glasses. Electrical studies on phase change memory (PCM) cells in the amorphous phase reveals that the sub-threshold current is due to a modified Poole-Frenkel (PF) transport mechanism. An analytical model is shown which is able to account for both the shape of the I-V characteristics and its temperature dependence. The significance of the sub-threshold slope for physical characterization of the trap concentration in the amorphous phase is shown. The sub-threshold conduction model is then extended to describe threshold switching, that is the abrupt increase of conductivity above a characteristic (threshold) point in the I-V curve. An analytical model is shown where threshold switching results from the energy gain of trapped carriers due to the high electric field, therefore resulting in the filling of high-mobility, high-energy traps. The analytical model for conduction and switching in PCM cells is able to reproduce I-V characteristics for different temperature and programmed states, allowing for fast, accurate and physics-based prediction of cell behavior at the array level.

Key words: chalcogenide glass, threshold switching, Poole-Frenkel transport.

1. INTRODUCTION

Sub-threshold conduction and threshold switching in chalcogenide glasses have attracted fundamental investigation since the early discovery of Stanford Ovshinsky in 1968 [1]. These materials display a large resistance at relatively low voltage, up to a certain condition called threshold voltage. As the voltage (or current) is increased above the threshold point, the conductivity is suddenly increased to a new, relatively large value. The large conductivity increase is generally accompanied by a voltage snap-back, resulting in the typical S-shaped negative differential resistance (NDR) behavior. A distinction can be made among chalcogenide materials, depending on the behavior during successive switching operation: *Threshold-switching* materials again feature a high resistance after the voltage and current are reduced to zero after threshold switching. On the other hand, *memory-switching* materials can be found in a low resistive state after switching, revealing the change of their structure from the amorphous to the crystalline phase as a result of the large Joule heating during threshold switching. This is at the basis of the PCM technology [2,3], where the threshold switching is the key electrical process allowing for current-induced phase change in nanometer scaled chalcogenide devices.

The physical interpretation of threshold switching in chalcogenide materials is, on one hand, a challenge from the fundamental standpoint, and, on the other, is a necessary step toward the development of accurate, physically-based models for PCM cell operation. For instance, the description and prediction of crystallization processes occurring during a 100ns current set pulse in a PCM cell would not be possible if the detailed dynamics and localization of the current during threshold switching is unknown. Also, the ability to predict the V_T for threshold switching is essential for designing the programming and read conditions in a PCM cell. Threshold switching was recognized to be an electronic process in nature [4-6]. However, the physical details of this mechanisms are still widely debated. Among the proposed mechanism to explain threshold switching, we recall thermal instabilities [7], impact ionization coupled with Shockley-Hall-Read recombination [4,5,8], polaron instability [9] and nucleation of crystalline phase [10]. In general, none of these models describe consistently and quantitatively both the sub-threshold conduction process and threshold switching within the same physical framework, and, at the same time, is able to predict the correct temperature and thickness dependence of sub-threshold conduction and threshold switching.

This paper will review recent progress [11-13] about the interpretation and modelling of sub-threshold conduction and threshold switching in chalcogenide glasses. Sub-threshold current is explained by trap-limited Poole-Frenkel (PF)

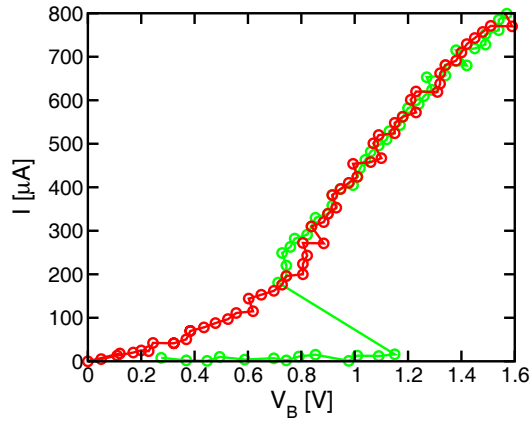


Fig. 1 Measured I-V curves for a PCM cell in the set (red) or reset (green) states. The latter displays the threshold switching process at about $V_T=1.2V$.

transport, while threshold switching is described by PF instability due to energy gain at relatively high field. The relevance of these new findings in terms of modelling of PCM cells and arrays will be highlighted.

2. EXPERIMENTS

Electrical measurements were conducted on PCM cells fabricated in a $0.18\ \mu\text{m}$ technology. These samples contains $\text{Ge}_2\text{Sb}_2\text{Te}_5$ (GST) as the active phase-change material. Fig. 1 shows typical I-V curves for the set and the reset state, corresponding to the crystalline and the amorphous phases in the GST, respectively. The set state features a non linear I-V curve with a low-current resistance R_{set} of about $5\text{k}\Omega$, and a dynamic resistance R_{on} of about $1\text{k}\Omega$. The transition from R_{set} to R_{on} can be explained by the cooperation of thermal effects, increasing the concentration of carriers through thermal generation in the small band-gap semiconductor (about $0.5\ \text{eV}$ for the crystalline phase of GST [8]) and field effects, increasing the concentration and mobility of carriers by impact ionization and PF mechanisms. The reset state is characterized by a larger resistance R_{reset} , usually in the range of few $\text{M}\Omega$. As a voltage $V_T=1.4V$ is reached, however, the material conductance suddenly switches to a high value, approximately corresponding to the same R_{on} observed for the set state at high currents. The sudden transition of conduction behavior is known as threshold switching, and is typical for many chalcogenide materials in their amorphous phase. Although in some chalcogenide glasses the threshold switching results in a transition from the amorphous to the crystalline phase, this is not the general case [14]. Therefore the threshold switching cannot be interpreted in terms of phase change, but is instead an electronic mechanism [4,6].

3. SUB-THRESHOLD CHARACTERISTICS

Threshold switching appears as an instability behavior taking place at a critical point along the sub-threshold regime. Therefore, for a thorough understanding of the switching process, the sub-threshold transport mechanism has to be explained first. To this aim, we shall consider the experimentally-measured I-V curves, shown in Fig.2 for a PCM cell with $\text{Ge}_2\text{Sb}_2\text{Te}_5$ (GST) chalcogenide material which was initially programmed in a reset state. Once observed on a logarithmic scale, the sub-threshold current reveals its specific dependence on voltage. The shape of the I-V curve indicate a linear behavior for very small voltage, while an exponential increase of current is observed at relatively large voltage. Incidentally, note that this voltage dependence may be reproduced mathematically by a hyperbolic sin (sinh) equation of the type: $I=I_0\sinh(BV)$ [11,13]. To gain more insight in the physical mechanism responsible for this voltage dependence, the temperature dependence of the current was analyzed in Fig. 1. A strong temperature activation of current can be seen, which can be explained by the intrinsic-semiconductor behavior of chalcogenide materials in the amorphous phase. In fact, the concentration of defects in chalcogenide glasses is so high that the Fermi level E_F is pinned to a deep position in the band gap. As a result, the activation energy for conduction, given by the

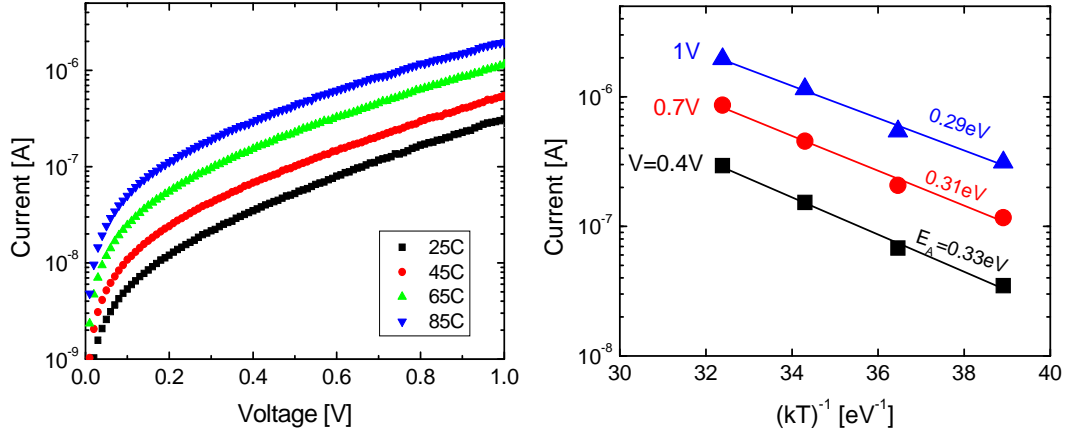


Fig. 2 Measured I-V characteristics in the sub-threshold regime for amorphous GST at increasing temperature (left) and Arrhenius plot of the current at increasing voltage (right).

difference between the conduction band level E_C and E_F in the case of dominant concentration of electrons in the material, is around half of the energy gap, which is about 0.7-0.8 eV for amorphous GST [8].

A more detailed analysis of the T-dependence of the current in the figure reveals that the activation energy $E_A = d \log I / d(1/kT)$ is a decreasing function of the applied voltage. This is clearly shown in Fig. 2 (right), where the current values measured at three different voltages $V=0.4, 0.7$ and 1 V are plotted as a function of $1/kT$. The activation energy resulting from the linear fitting in this Arrhenius plot decreases with voltage from 0.33 to 0.29 eV [11,12].

4. ANALYTICAL MODEL FOR SUB-THRESHOLD TRANSPORT

The decreasing activation energy shown in Fig. 2 has been widely observed to apply to materials where transport is controlled by traps in the forbidden gap [15]. Based on this indication, a new analytical model was developed in [11-13], which is schematically shown in Fig. 3. It is assumed that the current is due to a PF transport of electrons through traps, located at a distance Δz one from each other. When no voltage is applied, electrons have to overcome a potential barrier $\Delta\phi(0)$, by thermal emission (Fig. 3a). As a voltage is applied, the barrier for electrons is lowered to $\Delta\phi(V)$, resulting in an enhancement of the thermal emission probability over the barrier and, hence, of the forward current I_{\rightarrow} (Fig. 3b). The latter is defined as the current contribution due to electrons flowing in the same direction as the electrostatic force, i.e. opposite to the applied electric field, which can be written as:

$$I_{\rightarrow} = qAN_T \frac{\Delta z}{\tau_0} e^{-\frac{E_C - E_F - qV\Delta z/2u_a}{kT}}, \quad (1)$$

where A is the area of the contact of the active volume in the PCM cell, N_T is the total concentration of traps, τ_0 is the characteristics attempt-to-escape time of the electron and u_a is the thickness of the amorphous layer. Eq. (1) results from the integration of several contributions dI_{\rightarrow} , each corresponding to a trap energy differential dE_T [13]. In this equation, the potential barrier $\Delta\phi(V)$ is linearly decreasing with the applied voltage, which is the case for the small- Δz limit, in amorphous semiconductors with a large concentration of traps. On the other hand, for relatively large Δz (i.e. small N_T), the usual potential barrier lowering proportional to the square root of the voltage is observed [13]. The potential barrier in Eq. (1) was simply calculated as the conduction band level in correspondence of the middle point between the initial and the final localized state, at $\Delta z/2$ [13].

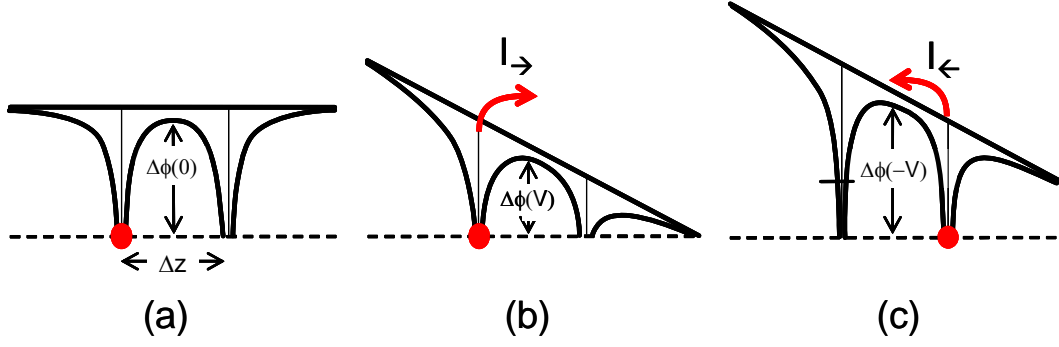


Fig. 3 Schematic for the analytical model for sub-threshold transport. The current is due to electron being emitted from one trapped state to another, over a potential barrier $\Delta\phi(0)$ at no applied voltage (a). As a voltage is applied, the barrier is lowered to $\Delta\phi(V)$, resulting in an exponential enhancement of the forward the current I_{\rightarrow} (b). The reverse contribution to the current I_{\leftarrow} must also be considered (c).

In addition to the forward current in Eq. (1), also the reverse contribution should be taken in to account in particular at low voltages (Fig. 3c). This is due to electrons being thermally emitted over the barrier toward a trap in the opposite direction of the electrostatic force. The potential barrier is increased in this case, by an amount $qV\Delta z/2u_a$, i.e. equal to the lowering for the forward current. Therefore the reverse current can be written as:

$$I_{\leftarrow} = qAN_T \frac{\Delta z}{\tau_0} e^{-\frac{E_C - E_F + qV\Delta z/2u_a}{kT}}, \quad (2)$$

the only difference from Eq. (1) being the reversed sign of the potential barrier change in the exponent. The total current can be calculated from the difference between I_{\rightarrow} [Eq. (1)] and I_{\leftarrow} [Eq. (2)], yielding:

$$I = 2qAN_T \frac{\Delta z}{\tau_0} e^{-\frac{E_C - E_F}{kT}} \sinh\left(\frac{qV \Delta z}{kT 2u_a}\right), \quad (3)$$

where the sinh function results from the difference between the two equal exponential terms, with opposite signs. It is this sinh-type voltage dependence which can account for the linear/exponential voltage dependence at low/high voltage in Fig. 2. From Eq. (3), two important parameters describing the exponential regime of the sub-threshold current can be calculated. These are the already mentioned activation energy:

$$E_A = \frac{d \log I}{d(1/kT)} = E_C - E_F - qV \frac{\Delta z}{2u_a}, \quad (4)$$

and the sub-threshold STS, defined as the derivative of the log of the current with respect of the voltage, and given by:

$$STS = \frac{d \log I}{dV} = \frac{q}{kT} \frac{\Delta z}{2u_a}. \quad (5)$$

It is clear from Eqs. (4) and (5) that both E_A and STS depend linearly on the microscopic parameters Δz and u_a , namely on the ratio between the average trap distance and the thickness of the amorphous layer.

5. EXPERIMENTAL EVIDENCE AND SIMULATION RESULTS

To confirm Eqs. (4) and (5) and the analytical model from which they were obtained, E_A and STS were extracted from experimental data in Fig. 2 [12]. Fig. 4 shows the measured activation energy as a function of the applied voltage (a) and the STS as a function of $1/kT$ (b). In both cases, calculated results from Eqs. (4) and (5) agree well with data for $\Delta z/u_a=0.17$. The consistent and independent indications from the analysis of the temperature dependence of current

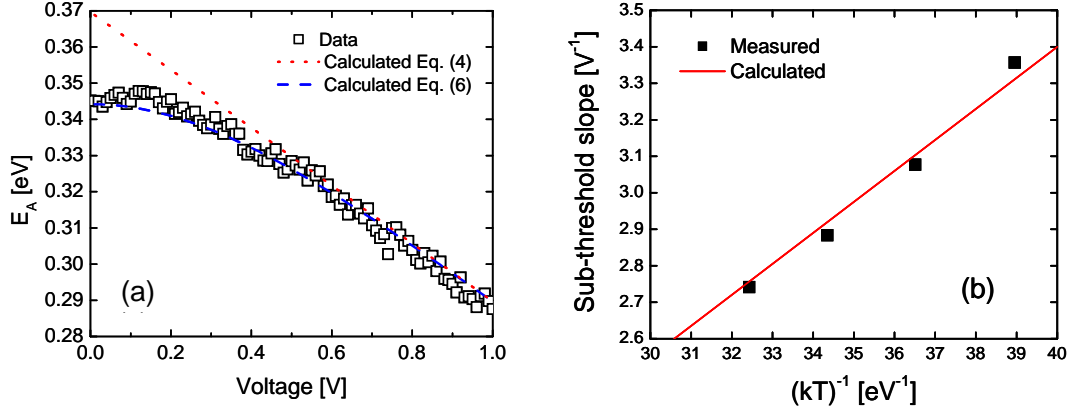


Fig. 4 Experimental activation energy E_A , as a function of voltage (a), and experimental STS as a function of $1/kT$ (b) Both figures also show calculations according to Eq. (4) and Eq. (5), assuming $\Delta z/u_a=0.17$. Also shown in (a) are the simulation results from the full analytical expression for E_A , from Eq. (6).

(E_A , Fig. 4a) and from the voltage dependence of current (STS, Fig. 4b) provide a strong support of the physical basis of the analytical model [12].

It is important to note that the activation energy in Fig. 4a is shown also for small voltages, in the linear region of the current, and not only in the exponential regime, where expression in Eq. (4) holds. To obtain a generally valid expression for the activation energy, the log of the total current in Eq. (3) has to be derived with respect to voltage, yielding:

$$E_A = E_C - E_F - \frac{qV_A}{kT} \coth\left(\frac{qV_A}{kT} \frac{\Delta z}{2u_a}\right). \quad (6)$$

Calculations according to Eq. (6) are shown in Fig. 4a, displaying a good agreement in both the linear (low-voltage) and exponential (high voltage) regimes. In particular, the model is able to reproduce the saturation of E_A at low voltage, where E_A tends to $E_C - E_F - kT$ for $V \rightarrow 0$ [13]. This results from the contribution of the reverse current, competing with the forward current and causing the apparent activation energy to be smaller than the real activation energy for the forward and reverse processes, each equal to $E_C - E_F$ for very small voltages. For large voltages, Eq. (6) is instead able to reproduce the linear voltage decrease of E_A already observed in Fig. 2.

Fig. 5 shows experimental and calculated I-V curves for increasing temperature. The good agreement in the figure demonstrates that the model correctly captures the essential physical nature of the sub-threshold transport in our samples.

6. THRESHOLD SWITCHING

As the field/current-density values in the chalcogenide material approach a critical condition along the sub-threshold characteristic, an instability process takes place, leading to a sudden increase of conductivity in the material. This can appear as a vertical increase of the current in correspondence of the threshold voltage V_T , if the voltage is forced directly across the cell during the measurement, or it can result in the typical voltage snap back, if the voltage is applied to the cell and a load resistor R_L in series to the cell [16]. The switching mechanism has raised an intense interest in terms of fundamental physics since its early discovery [1]. From the applicative point of view, threshold switching plays an essential role in the operation and performance of the PCM cell: in fact, the threshold voltage V_T

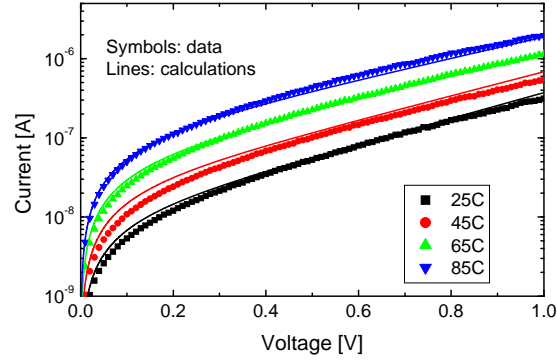


Fig. 5 Measured and calculated I-V curves for increasing temperature in the sub-threshold regime.

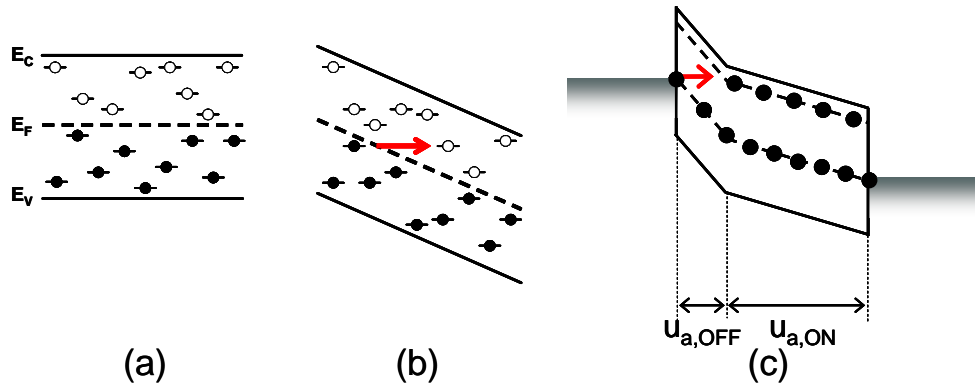


Fig. 6 Schematic for the injection process taking place at high-field and responsible for threshold switching in the amorphous phase of the chalcogenide material. (a) shows the equilibrium energy distribution of electrons at low field, while (b) show the field-induced gain process leading to a non-equilibrium electron distribution. Due to the presence of a dead space for electron energy gain $u_{a,OFF}$, the non-equilibrium distribution of electrons is maintained only in a portion $u_{a,ON}$ of the amorphous layer, resulting in a significant field non uniformity in the amorphous chalcogenide.

defines the boundary between the read voltage range and the programming voltage range, thus its stability and controllability in the PCM cell is vital. On the other hand, the switching time, which was estimated to be in the range of few hundreds of ps [4], represents the ultimate limit for the programming speed in the PCM and for the switching speed in ovonic threshold switches based on the same mechanism [14].

The conduction instability mechanism at the basis of threshold switching can be explained by the high-field PF process, schematically shown in Fig. 6. For low voltage, PF transport occurs maintaining the equilibrium energy distribution of electrons, namely a Fermi-Dirac distribution with a specific E_F level deep in the energy gap (a). For sufficiently high electric-field, electrons can gain a significant energy as a result of the applied field. This can be viewed as an injection mechanism occurring from low-energy to high energy localized states, as shown in Fig. 5b. A higher electron energy corresponds to a higher PF ‘mobility’, as a result of the decreased potential barrier for thermal emission, resulting in an increase of conductivity. However, the finite distance (off space $u_{a,OFF}$) for energy gain of electrons under the applied field should be considered, as shown in Fig. 5c. This results in a significant field non-uniformity in the amorphous layer: in fact, to maintain the same current, the electric field has to be very large in the low-conductivity, OFF space $u_{a,OFF}$, where the energy distribution is close to equilibrium, and very small in the high-

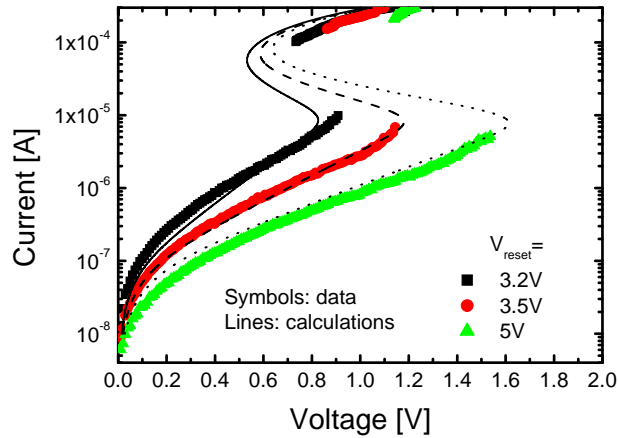


Fig. 7 Measured and calculated I-V curves for a PCM cell programmed at different voltages V_{reset} , corresponding to increasing thickness of the amorphous region in the cell.

conductivity ON layer $u_{a,\text{ON}}$, where electrons have a large average energy. The field collapse in the ON region results in the negative differential resistance (NDR) effect, appearing as a voltage snap back along the measured I-V curve.

Based on this physical picture, an analytical model was developed in [11,13] for threshold switching. The conduction model was the same as the PF equation of Eq. (3), except for the effective concentration of electrons and the corresponding energy contributing to the current. The energy gain process was modelled as a tunnelling injection from deep states, close to the E_F , to high-energy (shallow) states close to the conduction band E_C [11,13]. This approach allowed for the consistent calculation of the I-V curves for different programmed states (corresponding to different thickness of the amorphous layer u_a), as shown in Fig. 7. Calculations in the figure agree closely with data in both the sub-threshold region (low-voltage resistance, sub-threshold slope) and the switching parameters (threshold voltage, threshold current). The good agreement supports the physical basis on which the model was developed.

4. CONCLUSION

Recent results on the understanding and modeling of conduction and switching in amorphous chalcogenide materials for application in PCM devices were reviewed. An analytical model based on PF transport for sub-threshold transport accounts closely for the I-V characteristics, the voltage dependence of activation energy and the temperature dependence of sub-threshold slope. In the framework of the same PF conduction model, a switching model was presented, where switching is described by the non-uniform energy distribution of electrons as a result of field-induced energy gain. The analytical conduction/switching model is able to reproduce I-V characteristics for different temperature and programmed states, allowing for fast, accurate and physics-based prediction of cell behavior at the array level.

4. ACKNOWLEDGMENTS

The authors would like to thank Y. Zhang, D. Kau, G. Atwood and G. Spadini from Intel for precious discussions.

REFERENCES

1. S. R. Ovshinsky, *Phys. Rev. Lett.* **21** (1968) 1450.

2. S. Lai and T. Lowrey, *IEDM Tech. Dig.* (2001) 803.
3. S. Lai, *IEDM Tech. Dig.* (2003) 255.
4. D. Adler, M. S. Shur, M. Silver and S. R. Ovshinsky, *J. Appl. Phys.* **51** (1980) 3289.
5. D. Adler, H. K. Henisch and N. Mott, *Rev. Mod. Phys.* **50** (1978) 209.
6. A. Redaelli, A. Pirovano, F. Pellizzer, A. L. Lacaita, D. Ielmini and R. Bez, *IEEE Electron Device Lett.* **25** (2004) 684.
7. A. C. Warren, *IEEE Trans. Electron Devices* **20** (1973) 123.
8. A. Pirovano, A. L. Lacaita, A. Benvenuti, F. Pellizzer and R. Bez, *IEEE Trans. Electron Devices* **51** (2004) 452.
9. D. Emin, *Phys. Rev. B* **74** (2006) 035206.
10. V. G. Karpov, Y. A. Kryukov, S. D. Savransky, and I. V. Karpov, *Appl. Phys. Lett.* **90** (2007) 123504.
11. D. Ielmini and Y. Zhang, *IEDM Tech. Dig.* (2006) 401.
12. D. Ielmini and Y. Zhang, *Appl. Phys. Lett.* **90** (2007) 192102.
13. D. Ielmini and Y. Zhang, *J. Appl. Phys.* **102** (2007) 054517.
14. S. Prakash, S. Asokan and D. B. Ghare, *IEEE Electron Device Lett.* **18** (1997) 45.
15. C. B. Thomas, *J. Phys. D* **9** (1976) 2587.
16. D. Ielmini, A. L. Lacaita and D. Mantegazza, *IEEE Trans. Electron Devices* **54** (2007) 308.